Novel dual microelectrode probe for the simultaneous visualization of local Zn^{2+} and pH distributions in galvanic corrosion processes

D. Filotás[1,2], B.M. Fernández-Pérez[3], J. Izquierdo[3,4], L. Nagy[1,2], G. Nagy[1,2,*], R.M. Souto[3,4,*]

[1] *Department of General and Physical Chemistry, Faculty of Sciences, University of Pécs, Ifjúság útja 6, 7624 Pécs, Hungary.*
[2] *János Szentágothai Research Center, University of Pécs, Ifjúság u. 20. Pécs, 7624 Hungary.*
[3] *Department of Chemistry, Universidad de La Laguna, P.O. Box 456, E-38200 La Laguna, Tenerife, Canary Islands, Spain.*
[4] *Institute of Material Science and Nanotechnology, Universidad de La Laguna, E-38200 La Laguna (Tenerife), Spain.*

Abstract

Novel dual potentiometric microsensor probe has been developed for the simultaneous detection of Zn^{2+} concentration and pH distributions in the Scanning Electrochemical Microscopy investigation of corroding galvanized steel. The individual sensors show nearly theoretical behavior over a wide concentration range. The applicability of this probe is first demonstrated on a Fe-Zn galvanic couple, as it shows excellent performance in these simultaneous model experiments. In addition, linear scans recorded over a cut edge of coated galvanized steel evidences the complementary information gathered on the electrochemical behavior of the corroding sample, and adumbrates promising and feasible applications of multi-barrel microelectrodes in corrosion research.

Keywords: Iron; Zinc; Scanning electrochemical microscopy; Ion selective microelectrode; Galvanic corrosion; Local pH distribution.

1. Introduction

The acquisition of spatially-resolved information from corrosion processes is crucial for the development of efficient protection methods. Therefore, surface scanning techniques with electrochemical resolution such as the scanning vibrating electrode technique (SVET)), the scanning ion-selective electrode technique (SIET) and scanning electrochemical microscopy (SECM) are becoming essential tools in this field [1-4]. In general, amperometric microelectrodes are the usual sensing probes in SECM studies [2,4], though spatially-resolved pH measurements also provide information regarding the allocation of anodic and cathodic regions [5]. Besides micropipette type pH sensors [6], miniaturized metal/metal oxide type electrodes have been employed in local pH measurements [7-9]. On the other hand, Mg^{2+} and Zn^{2+} ion-selective microelectrodes (ISME) have also been employed as SECM and SIET sensing probes in galvanic corrosion studies [10-14]. As a result, various probes are currently available for operation in SECM, though their combined use for the characterization of a given corrosion process usually implies probe exchange. The latter severely limits the precision of the measurement device as to image the same spot on the substrate, and prevents simultaneous in situ characterization of these dynamic systems. Alternately, the use of two probe holders has enabled the simultaneous acquisition of two concentration profiles for ions of interest. In this case, two different selective probes were positioned in close proximity with the aid of high-gain videocameras, and they were simultaneously scanned across the surface [15]. Unfortunately, this approach exhibits the disadvantage of employing two individual probes instead of one, enhancing the convective effects due to the motion of the microelectrodes while measuring, and demanding reproducible control of the inter-electrode distance by the operator.

These drawbacks can be better addressed using multi-barreled microelectrodes similar to those employed in iontophoresis applications by life scientists [16-19]. Though a multi-channel assembly containing a gallium microelectrode was employed in potentiometric SECM studies for setting the tip-sample distance about 20 years ago [20], multi-barreled electrodes have not been employed in SECM investigations for the simultaneous visualization of the local concentration distributions of two ionic species produced during the complex corrosion processes until now. To the best of our knowledge, the only progress has been produced by Lamaka and coworkers for the quasi-simultaneous monitoring of ionic current, pH and O_2 concentration using SVET [21,22].

In this paper we describe the fabrication of a dual microelectrode probe for the application of potentiometric SECM to the in situ study of localised corrosion processes. In particular, this work focuses on the preferential dissolution of zinc versus more noble metals, a protection strategy widely exploited especially for steel, since galvanized steel sheet with organic coating is regarded to offer an excellent corrosion resistance for the automobile and building industries. Although, the sacrificial anodic protection of zinc is well known, in the case of galvanized metals, due to the very low zinc/steel ratio, this cannot be regarded as the sole mechanism. More likely, the formation of zinc corrosion products on the steel surface is responsible for the receded corrosion activity [23-28]. However, the buried steel matrix can be accidentally exposed to the corrosive environment. Scratches and cut edges are the main undesirable failure modes of these materials, and therefore attract major research interest towards their prevention [29-35]. The ability of the double-barrel microelectrode assembly to simultaneously image Zn^{2+} ion and pH concentration distributions has been tested over an iron-zinc model galvanic couple, and over a cut edge of coil-coated galvanized steel. Both systems were already characterized using both amperometric and potentiometric operations in SECM, though using single probes (i.e., the interested reader is referred to refs. [9-13] in the case of the model Fe-Zn galvanic couple, and refs. [36,37] for the cut edge of coil coated galvanized steel). We demonstrate that the new experimental approach proposed here efficiently distinguishes domains with different electrochemical activity in galvanic corrosion reactions and allow simultaneous quantification of the ionic species participating in the processes.

2. Experimental

Experiments were performed on two different samples, namely a model Fe-Zn sample and a cut edge of coated galvanized steel. The Fe-Zn galvanic pair sample was prepared by embedding 1-mm diameter Zn and Fe wires (> 99.5 % purity, Goodfellow, Cambrdidge, UK) into Epofix resin sleeve (Struers, Ballerup, Denmark) with 1 mm separation between them resulting in a similar assembly to those used in previous reports [9,13]. The electric contact of the wires protrudes at the rear of the mold allowing electric connection between the metals. The top side was thoroughly wet ground and polished using a sequence of abrasive papers and alumina slur with decreasing grit size (down to 2.5 μm) and

particle size (down to 0.05 μm), respectively. Finally, the Fe-Zn sample was rinsed with acetone and ultra-pure water purified by Milli-Q system from Millipore (18 MΩ cm). The second experimental system was the cut edge of painted galvanized carbon steel, previously characterized in similar configuration using amperometric SECM operated in the feedback mode, as well as pH sensors [36,37]. The thickness of the steel foil was 400 μm, while the galvanized layer was 25 ± 5 μm electrodeposited zinc. A 5 μm thick polyester primer was applied to both sides of the galvanized steel foil, whereas a single 20 μm thick polyester topcoat containing TiO_2 was applied only to one side. Samples were cut with a guillotine and embedded into Epofix resin.

EDOT (3,4-ethylenedioxythiophene) purchased from HC Starck GmbH (Goslar, Germany) was used for the preparation of the solid PEDOT (poly-3,4-ethylenedioxythiophene) contact on carbon fibre of 30 μm diameter (obtained as a generous gift from Specialty Materials, Lowell, Massachusetts, USA) in Zn(II) ion-selective microelectrodes. Zinc ionophore I, and all membrane components were supplied by Sigma Aldrich. The 1-butyl-3-methylimidazolium hexafluorophosphate ($BMIM^+$ PF_6^-) ionic liquid was purchased from Fluka. The silanizing solution was 5% dichloro-dimethyl silane in heptane, supplied by Fluka.

The novel dual Zn^{2+}/pH selective microelectrode probe is sketched in Figure 1A. Borosilicate capillaries, with inner and outer diameter of 1.0 and 0.79 mm, respectively, were supplied by Hilgenberg GmbH (Malsfeld, Germany). First, borosilicate capillaries were soaked in 1:1 mixture of concentrated H_2SO_4 and 30% H_2O_2 solutions, and then thoroughly rinsed with Milli-Q water. The capillaries were then held together, and subjected to a twist-and-pull procedure using a Narishige PE-2 instrument (Tokyo, Japan). In the first step, the capillaries were carefully soften and twisted, resulting in two intertwined capillaries with approximately the original dimensions. After cooling, the double-barrel capillaries were pulled through a second heating process, rendering the pulled shape shown in Figure 1B-C. The inner walls of the capillaries were next hydrophobized by dipping the tips into the silanization solution. The preparation of the solid contact Zn-ISME barrel next consisted in the electrochemical polymerization of PEDOT on a 30 μm diameter carbon fiber. About 1-2 cm long carbon fiber was employed, and attached to a copper wire with silver epoxy adhesive. The wire was used as working electrode in 0.1 molar EDOT-containing $BMIM^+$ PF_6^- ionic liquid solution with silver reference and platinum auxiliary electrodes. In the polymerization step, 10 consecutive cyclic voltammetry cycles were taken in $-0.9 \leq E \leq 1.3$ V range. The PEDOT coated carbon fiber was doped

in 0.1 M KCl aqueous solution through the application of 15 consecutive potential cycles in the $-0.9 \leq E \leq 0.8$ V range. In the same solution, the performance of the obtained coating was tested by cyclic voltammetry, in the $-0.4 \leq E \leq 0.5$ range, 5 consecutive scans were taken (not shown). All the cyclic voltammetric treatments were performed at 0.05 V s^{-1} scan rate. The cocktail contains 98 mg tetrahydrofuran, 42 μL 2-nitrophenyl-octyl ether emollient, 2.26 mg PVC, 0.99 mg ionophore, 0.22 mg potassium-[tetrakis-4-chlorophenyl]-borate. Finally, the PEDOT coated carbon fiber was inserted in the lumen of the capillary and pushed as close as possible to the orifice of the tip.

The preparation of the antimony electrode preparation was adapted from a procedure described elsewhere [7]. Molten antimony was introduced into a capillary by applying vacuum on the other end. Then, microwires were pulled together with the glass in a flame using tweezers. Appropriate, 1-3 cm sections were chosen and adjusted to the orifice of the tip next to the Zn-ISME barrel. The electric contact copper wire was provided either using mercury (see Figure 1A) or glued with silver epoxy. The micrograph in Figure 1 shows the tip of a typical tip of the dual microelectrode probes. The carbon fiber for the solid contact Zn-ISME was pushed towards the orifice of the corresponding barrel, thereby placed as close as possible to the end of the capillary (ca. 200-300 μm) with shrinking inner diameter. Typically, the diameter of the orifices of the individual barrels amounted 10-20 μm, whereas the diameter of the resulting active antimony disc was 5-10 μm. The distance between the two barrels was usually 10-15 μm measured from the edges of the active areas (namely, antimony disc and ionophore cocktail). The calibration of the Zn-sensitive barrel was carried out in x M $ZnSO_4$ + 10^{-3} M NaCl in aqueous solutions ($10^{-1} \geq x \geq 10^{-6}$). The antimony electrode was successively immersed in $4 \leq pH \leq 10$ Britton Robinson buffers (the pH of the buffers was checked with combined glass electrode), and its potential was measured against an Ag/AgCl/KCl (3.5 M) reference electrode.

In order to determine the selectivity coefficients for the as-prepared Zn-ISME in the dual probe, expressed in terms of the $\log(K_{ij}^{pot})$ values, the separate solution method (SSM) was applied for Na^+, Fe^{2+} and Fe^{3+}. The same calibration method was carried out in the series of the solutions of the interfering ions, as it was in case the primary ion (Zn^{2+}). The solutions of the metal ions where prepared from their chloride and sulfate salts obtained from Reanal (Budapest, Hungary) or Sigma Aldrich. As it is well known, $\log(K_{ij}^{pot})$ can be defined as [38]:

$$\log(K_{ij}^{pot}) = \left(E_j^0 - E_i^0\right)\frac{z_i F}{2.303RT} + \left(1 - z_i/z_j\right)log(a_i) \quad (1)$$

where E_j^0 and E_i^0 are the individual potentials of the interfering (*j*) and primary (*i*) ions extrapolated to a_i = 1 M activity; z_j and z_i are the charges of the interfering (*j*) and primary (*i*) ions; *F*, *R* and *T* have their usual meanings.

Potentiometric SECM measurements have been carried out in a homemade instrument operated with custom software allowing high scan rates and arc scanning pattern. The local potential values measured against a single Ag/AgCl/KCl (3.5M) reference electrode have been registered using an isoPod type high input impedance mV/pH meter with an e-corder data acquisitioning device and an USB-isoPod type voltmeter connected directly to the computer. The mV/pH meters and the data acquisitioning device were purchased from eDAQ (Denistone East, Australia).

In order to establish the contribution of the electric field in the potentiometric response of the Zn-ISME, the electrode probe was scanned in the vicinity of a point source of electric field with controlled current flow. This was done by employing a pipette electrode filled with 1 mM NaCl testing solution as the current source and a platinum wire separated ca. 1 cm from the orifice. Another platinum wire was used as auxiliary electrode in the bulk of the cell, filled with the same testing solution. The Zn-ISME was scanned across the end of the pipette at 100 μm height, while forcing a current flow through the two electrodes by inter-connecting them at the rear part with a 6 V battery, controlled with resistors connected in series. The resistors were selected in the kΩ to MΩ range.

3. Results and discussion

3.1 Characterization of the electrochemical behavior of the ISME in the double barrel probe

Simultaneous monitoring of pH and Zn^{2+} concentration over corroding samples using SECM can be performed using this double-barrel ion selective microelectrode arrangement. Typical calibration curves of the individual ISME in the combined probe are depicted in Figure 2. The two systems exhibit extensive linearity ranges covering several ten powers for the activities of both hydrogen and zinc ions, expressed as pH and pZn (where $pZn = -\log a_{Zn^{2+}}$), respectively. The slope obtained for the Zn^{2+}-ISME in the $1 \leq$ pZn ≤ 5 range is very close to the theoretical value 29.58 mV decade^{-1} for divalent ions, whereas a sub-Nernstian behavior was found for the antimony microelectrode, a feature previously reported for other antimony electrodes based on polycrystalline and amorphous Sb/Sb_2O_3

surface [5,9,14,36,37].

The selectivity of the Zn ISME against other possible interfering metals was tested using the SSM method. It was applied for Na^+, Fe^{2+} and Fe^{3+}, and the obtained $\log(K_{ij}^{pot})$ values are given in Table 1. For the sake of comparison, the selectivity coefficients provided by Fluka for sodium and iron ions for the recommended optimized cocktail composition for macroelectrodes are also given in the table. In spite of the different composition of the herein employed ionophore for micrometer-sized membranes with respect to the recommendation from the manufacturer (i.e., more fluid cocktails are needed to introduce them inside the capillary), no major differences were observed in the selectivity coefficients, providing acceptable values for its application in the current studies. In addition, the pH dependence of the Zn ISME was determined by measuring the potential in buffers covering the $4 \leq pH \leq 10$ range, and practical problems were only observed in alkaline media (pH > 8) due to the insufficient solubility of the zinc hydroxides [39].

The model iron-zinc galvanic pair, built using two wires of the metal embedded in an insulating resin [9,13], was the first system chosen for the characterization of the new dual ion-selective probe arrangement. The physical separation of the two metals in the sample would allow the anodic and cathodic areas to be investigated separately, as well as to hinder any eventual chemical reactions in the solution phase between the products formed in the two half-cell reactions to occur over the metal wires. The anodic reaction in a Zn-Fe galvanic pair is the dissolution of Zn according to:

$$Zn \rightarrow Zn^{2+} + 2e^- \quad (2)$$

whereas the reduction of dissolved oxygen occurs on the surface of iron:

$$O_2 + 2H_2O + 4e^- \rightarrow 4OH^- \quad (3)$$

Released zinc (II)-ions may undergo hydrolysis producing either the zincyl-ion or insoluble $Zn(OH)_2$ depending on the local pH:

$$Zn^{2+} + H_2O \rightleftarrows Zn(OH)^+ + H^+ \quad (4)$$

$$Zn(OH)^+ + H_2O \rightleftarrows Zn(OH)_2 + H^+ \quad (5)$$

$Zn(OH)_2$ can further form ZnO, or even $Zn(OH)_3^-$ and $Zn(OH)_4^-$ at higher pH values [39]. For our purpose, this means that the relative ratio of zinc-hydroxyl complexes might eventually compromise the analysis of the Zn^{2+} at pH values over 7, and insolubility of the zinc species is expected to affect at

pH values higher than 8.5 [39]. Besides, other side reactions may influence the quantitative determination of zinc (II) cations in the presence of chloride or carbonate [40].

In order to produce the galvanic coupling of iron and zinc, the metal wires should be electrically connected at the rear of the mould before the measurement. In this configuration, it was noticed that the electric field generated by the galvanic pair affects the potential signals of the ISME. If the contribution of the electric field to the potentiometric signal were ignored, misleading results would eventually be recorded. For instance, the Zn-ISME monitored almost one decade decrease of Zn^{2+} activity over the cathode compared to the bulk solution. Therefore, the pH dependence of the potential of the Zn-ISME was investigated (not shown), and it was observed to deliver negligible potential change in the $7 \leq pH \leq 9$ range, despite the proximity of the solution to cathodic areas. On the other side, when the galvanic pair was disconnected during the measurement, an instantaneous change of the potential could be observed. Effects due to the electric field have been previously observed and reported by the authors when using similar experimental set-ups, and already demonstrated to produce negligible variations in the registered potential [41]. Therefore, the possible effect of electric field on the Zn-ISME built in the dual probe arrangement was explored using the same strategy, as explained in the experimental section. That is, the Zn-ISME was scanned over a point source of an electric field during the application of progressively increasing currents. The obtained response is displayed in Figure 3. Results indicate that at least 3-4 μA should be flowing through the system for the electric field generated from a point source to be sensed by the ISME. This current value is, as it will be shown below, approximately ten times bigger than those recorded during the galvanic corrosion of the Fe-Zn galvanic couple.

Finally, cross-talk effects were evaluated by simply scanning over the FeZn surface under galvanic coupling with simultaneous and independent potential data acquisition of the two barrel-channels, thus finding no influence in their response due to the recording of the other channel.

*3.2. Monitoring of the model Fe-Zn galvanic couple*The dual probe ISME assembly was employed to monitor the model Fe-Zn galvanic couple, a system previously characterized using each ISME built as individual single-barrel electrodes under galvanic coupling [9,13]. By using the arc scanning algorithm described elsewhere [42], the concentration maps in the galvanic pair arrangement could be recorded at a relatively high scan rate (namely 100 μm s^{-1}) right after disconnection of the

galvanic pair, avoiding time-dependent image artifacts. Initially, the tip was positioned to the center of the levelled sample by visual observation, and then the tip-sample vertical distance was adjusted at 50 μm. The orifice sizes of the tips were always kept smaller than 20 μm, therefore the overall diameter of the probe never exceeded 40 μm. Consequently, for a typical 50 μm scanning step size, the signals recorded from both ISME in each measuring single step not only were actually simultaneous, but both concentration data could be effectively corresponded to the same space coordinates, which is a remarkable advance compared to previous quasi-simultaneous reports in the literature [21,22], and it is a more robust configuration compared to simultaneous potentiometric measurements by simultaneously produced by holding and scanning two probes in separate holders [15].

Figures 4 and 5 demonstrate how the dual microelectrode probe can be employed to visualize concentration distributions for zinc and hydrogen ions over a Fe-Zn galvanic couple immersed in 1 mM NaCl solution at ambient temperature. This low electrolyte concentration was selected in order to slow down the corrosion process and enable the evaluation of its early stages. The two metal wires were separated approximately 1 mm. In order to completely eliminate the contribution of the electric field during the measurements, the iron and zinc samples were left galvanically coupled for 30 min while immersed in the test solution (with typical current values of 0.4-0.5 μA flowing through the two metal surfaces), and they were only disconnected just before starting to record the corresponding potentiometric SECM scans. Owing to the high scan rate and the relatively long coupling time, it is assumed that (almost) invariant conditions in the vicinity of the sample in the quiescent solution are maintained throughout the scan.

The simultaneously recorded images for Zn^{2+} and pH distributions related to Fe-Zn galvanic coupling together with a micrograph of the Zn sample are depicted in Figure 4. The 2D scans nicely match the theoretical expectations. Above the zinc anode, the local activity of the zinc (II) ion increased up to the sub-milimolar range (see Figure 4B), while a weak acidification, close to one pH unit, could be observed as the side product of hydrolysis (Figure 4A). Similar features have been observed with the same surface undergoing sacrificial dissolution while monitored using single-barrel electrodes [9,13]. Although the cross sections of the metal wires are not perfect circles, the recorded pH and pZn maps still show this symmetry. The small distortion is due to the high scanning rate employed to minimize the effect of time when dynamic systems such as corroding samples are studied. In addition, it must be noticed that they were recorded using the fastest scanning pattern that consists in initiating

each successive line from the last coordinate reached in the previous line (i.e., effectively describing a zig zag trajectory, usually known as meander mode), that usually gives result to a more distorted image when recorded in the potentiometric mode. Analogously, Figure 5 shows the pH and Zn^{2+} distributions simultaneously monitored above the iron cathode. No significant variation in the Zn^{2+} concentration data was recorded over iron as it should be expected, despite the above-mentioned undesirable effect caused by the electric field when the iron and zinc were connected during the scan. Only small potential variations of ca. 10 mV could be detected, most probably arising from local fluctuations in Na^{+} concentration and the alkaline pH. Indeed, no abrupt variation in the recorded signal occurred when the sensing probe moved away from the iron sample into the surrounding resin. Only the rapid change of pH has a negligible effect on the apparent Zn^{2+}. By contrast, a large change in pH can be observed in Figure 5B measured with the antimony tip of the dual ISME probe as the consequence of the dissolved oxygen depletion in the cathodic half-cell reaction. This evident effect was about 2 pH units lower than those previously observed for the same surface under cathodic-protection [9], possibly as a result of the rapid diffusion of protons once the galvanic connection is interrupted prior to scans.

3.3. Monitoring of the cut edge of a painted galvanized steel system

In a second series of experiments, the cut edge of painted galvanized steel was considered to explore the applicability of the dual ion selective microelectrode probe for SECM studies. The cut edge of the coil coated steel was considered a practical system for investigation due to its broad-scale industrial application and relevance, while forming a limiting case of galvanic coupling in which a highly dissimilar surface ratio between the two metals was formed. The cross section of the painted galvanized steel foil was exposed to the test electrolyte. In this case, the anodic and the cathodic regions are located very close to each other, and as result local pH changes develop abruptly across the surface. That is, the Zn^{2+} ions produced in the anodic reaction can form $Zn(OH)_2$ and will eventually precipitate on the steel surface.

Line scans were recorded starting the tip movement from a location above the resin and passing over the zinc layer, the mild steel, zinc layer on the other side and stopping above the resin in the opposite side. The step size was 50 μm, the vertical tip-substrate distance was 50 μm and the overall traveled length was 2000 μm at a scan rate of 50 μm s^{-1}. Only line scans at a smaller scan rate were recorded because no scanning algorithms could be employed for this specific geometry in order to

minimize image artifacts related to higher scan rates. A selection of line scans are shown in Figure 6A-B, displaying both the pH and Zn^{2+} concentration distributions simultaneously recorded by means of the novel dual probe. The approximate location of the line scans and the scan direction are depicted on the micrograph in Figure 6C. The presented lines were selected from the area where significant anodic activity could be detected therefore the pH and pZn profiles can be compared. The behaviour of the surface was found to be heterogeneous over the whole area, with a pH distribution extending between 3.5 and 12 (not shown), similarly to previous observations [36,37]. Figure 6A shows that Zn^{2+} dissolution occurs on both sides of the cut edge, yet the anodic activity on the right side decreases from curve 1 (black coloured and rectangles) to curve 6 (olive and triangles). This feature can be explained on the basis of the information provided by the corresponding pH scans. A small acidification is observed above the zinc layer located at the left side of the cut edge, whereas pH increases above the mild steel foil as result of the oxygen reduction reaction. Similar concentration distributions have been previously seen, and their dynamic evolution evidenced [36]. With the herein gathered information, such evolution can be better understood. The alkaline area is located closer to the right side of the cut edge, therefore the pH in the neighborhood of the right anodic area is increasing from pH = 7.3 to 8.1. Considering the stability of the zinc-hydroxyl complexes the mole fraction of the Zn^{2+} ions decreases steeply along this pH interval [39]. That is, pZn lines 4,5 and 6 (cyan, magenta and olive) on the right side also reveal anodic activity however, the product of the reaction forms insoluble hydroxide precipitate in the vicinity of the cathodic area. Since the zinc ISME only detects Zn^{2+}, the observed decrease of the signal compared to the other side of the cut edge, where apparently constant anodic activity is observed, can be attributed to the precipitation of corrosion products. This perception does not depend on the scanning direction. This is an interesting example of the complementary information obtained with the simultaneous measurement, and opens a very promising route to the study of corrosion processes at cut edges, because zinc dissolution usually occurs through the formation of zinc basic salts or an oxide film depending on the actual local pH [43]. Though protective barrier skills are provided by the basic zinc salts [26,44], alkalization above pH = 9 leads to its transformation into zinc oxide [24], thus greatly affecting the corrosion corrosion efficiency of the galvanization layer towards protection of the buried steel.

4. Conclusions

In this work, a novel dual probe is presented for the simultaneous measurement of local Zn^{2+} and pH distributions in corrosion processes using SECM. The preparation of the probe attempted to produce individual ISME in the combined probe that will exhibit at least the same performance as those fabricated as a single-barrel. Data obtained for a model galvanic Fe-Zn system replicate previous observations made using separate single probes, yet allowing two concentration distributions to be recorded in one single experiment without cross-talking effects. A more complex system, namely a cut edge of painted galvanized steel was also successfully imaged with SECM, despite its unfavorable low Zn:Fe area ratio. The results described here demonstrate promising applicability of the novel multi-barrel SECM microprobes for simultaneous detection, as they would provide valuable in situ information to understand the behavior of complex corroding systems.

Acknowledgements

D. Filotás acknowledges a 2-month mobility grant to the University of La Laguna funded by the ERASMUS+ programme, and B.M.F.-P. thanks the Canary Agency for Research, Innovation and Information Society (Las Palmas de Gran Canaria, Spain) and the European Social Fund (Brussels, Belgium) for a research contract. Financial support by the Spanish Ministry of Economy and Competitiveness (MINECO, Madrid, Spain) and the European Regional Development Fund (Brussels, Belgium) under grant CTQ2016-80522-P is also acknowledged.

References

[1] R. Scott Lillard, Scanning electrode techniques for investigating near-surface solution current densities, in: P. Marcus, F. Mansfeld (Eds.), Analytical Methods in Corrosion Science and Engineering, CRC Press, Boca Raton, 2006, p. 571.

[2] R.M. Souto, S.V. Lamaka, S. González, Uses of scanning electrochemical microscopy in corrosion research, in: A. Méndez-Vilas, J. Díaz (Eds.), Microscopy: Science, Technology,

Applications and Education, Vol. 3, Formatex Research Center, Badajoz (Spain), 2010, p. 1769.

[3] S.V. Lamaka, R.M. Souto, M.G.S. Ferreira, In situ visualization of local corrosion by scanning ion-selective electrode technique (SIET), in: A. Méndez-Vilas, J. Díaz (Eds.), Microscopy: Science, Technology, Applications and Education, Vol. 3, Formatex Research Center, Badajoz (Spain), 2010, p. 2162.

[4] M.B. Jensen, D.E. Tallman, Application of SECM to corrosion studies, in: A.J. Bard, C. Zoski (Eds.), Electroanalytical Chemistry: A Series of Advances, Vol. 24, CRC Press, Boca Raton, 2012, p. 171.

[5] R.M. Souto, J. Izquierdo, J.J. Santana, A. Kiss, L. Nagy, G. Nagy, Progress in scanning electrochemical microscopy by coupling potentiometric and amperometric measurement modes, in: A. Méndez-Vilas (Ed.), Current Microscopy Contributions to Advances in Science and Technology, Vol. 2, Formatex Research Center, Badajoz (Spain), 2012, p. 1407.

[6] E.A. Zdrachek, A.G. Karotkaya, V.A. Nazarov, K.A. Andronchyk, L.S. Stanishevskii, V.V. Egorova, M.G. Taryba, D. Snihirova, M. Kopylovich, S.V. Lamaka, H^+-selective microelectrodes with optimized measuring range for corrosion studies, Sensor. Actuat. B-Chem. 207 (2015) 967-975.

[7] K. Tóth, G. Nagy, C. Wei, A. J. Bard, Novel application of potentiometric microelectrodes - scanning potentiometric microscopy, Electroanalysis 7 (1995) 801-810.

[8] B.R. Horrocks, M.V. Mirkin, D.T. Pierce, A.J. Bard, G. Nagy, K. Tóth, Scanning electrochemical microscopy. 19. Ion-selective potentiometric microscopy, Anal. Chem. 65 (1993) 1213-1224.

[9] J. Izquierdo, L. Nagy, Á. Varga, J.J. Santana, G. Nagy, R.M. Souto, Spatially resolved measurement of electrochemical activity and pH distributions in corrosion processes by scanning electrochemical microscopy using antimony microelectrode tips, Electrochim. Acta 56 (2011) 8846-8850.

[10] A.C. Bastos, M.G. Taryba, O.V. Karavai, M.L. Zheludkevich, S.V. Lamaka, M.G.S. Ferreira, Micropotentiometric mapping of local distributions of Zn^{2+} relevant to corrosion studies, Electrochem. Commun. 12 (2010) 394-397.

[11] S.V. Lamaka, O.V. Karavai, A.C. Bastos, M.L. Zheludkevich, M.G.S. Ferreira, Monitoring local spatial distribution of Mg^{2+}, pH and ionic currents, Electrochem. Commun. 10 (2008) 259-262.

[12] S.V. Lamaka, M.G. Taryba, M.L. Zheludkevich, M.G.S. Ferreira, Novel solid-contact ion-

selective microelectrodes for localized potentiometric measurements, Electroanalysis 21 (2009) 2447-2453.

[13] J. Izquierdo, L. Nagy, A. Varga, I. Bitter, G. Nagy, R.M. Souto, Scanning electrochemical microscopy for the investigation of corrosion processes: Measurement of Zn^{2+} spatial distribution with ion selective microelectrodes, Electrochim. Acta 59 (2012) 398-403.

[14] J. Izquierdo, L. Nagy, I. Bitter, R.M. Souto, G. Nagy, Potentiometric scanning electrochemical microscopy for the local characterization of the electrochemical behaviour of magnesium-based materials, Electrochim. Acta 87 (2013) 283-293.

[15] O.V. Karavai, A.C. Bastos, M.L. Zheludkevich, M.G. Taryba, S.V. Lamaka, M.G.S. Ferreira, Localized electrochemical study of corrosion inhibition in microdefects on coated AZ31 magnesium alloy, Electrochim. Acta 55 (2010) 5401-5406.

[16] D.C. Havey, D.M Caspary, A simple technique for constructing 'piggy-back' multi barrel microelectrodes, Electroen. Clin. Neuro. 48 (1980) 249-251.

[17] E. Ujec, E.E.O. Keller, N.K.V. Pavlík, J. Machek, Low-impedance, coaxial, ion-selective, double-barrel microelectrodes and their use in biological measurements, Bioelectroch. Bioener. 7 (1980) 363-369.

[18] D.J. Walker, S.J. Smith, A.J. Miller, Simultaneous measurement of intracellular pH and K^+ or NO_3^- in barley root cells using triple-barreled, ion-selective microelectrodes, Plant Physiol. 108 (1995) 743-751.

[19] K. Inagaki, S.A. Heiney, P.M. Blazquez, Method for the construction and use of carbon fiber multi barrel electrodes for deep brain recordings in the alert anal, J. Neurosci. Meth. 178 (2009) 255-262.

[20] C. Wei, A.J. Bard, I. Kapui, G. Nagy, K. Tóth, Scanning electrochemical microscopy, 32. Gallium ultramicroelectrodes and their application in ion selective probes, Anal. Chem. 68 (1996) 2651-2656.

[21] S.V. Lamaka, M. Taryba, M.F. Montemor, H.S. Isaacs, M.G.S. Ferreira, Quasi-simultaneous measurements of ionic currents by vibrating probe and pH distribution by ion-selective microelectrode, Electrochem. Commun. 13 (2011) 20-23.

[22] M.G. Taryba, M.F. Montemor, S.V. Lamaka, Quasi-simultaneous mapping of local current density, pH and dissolved O_2, Electroanalysis 27 (2015) 2725-2730.

[23] M. Mokaddem, P. Volovitch, K. Ogle, The anodic dissolution of zinc and zinc alloys in alkaline solution. I: Oxide formation on electrogalvanized steel, Electrochim. Acta 55 (2010) 7867-7875.

[24] J.D. Yoo, P. Volovitch, A. Abdel Aal, C. Allely, K. Ogle, The effect of an artificially synthesized simonkolleite layer on the corrosion of electrogalvanized steel, Corros. Sci. 70 (2013) 1-10.

[25] R.M. Souto, B. Normand, H. Takenouti, M. Keddam, Self-healing processes in coil coated cladding studied by the scanning vibrating electrode, Electrochim. Acta 55 (2010) 4551-4557.

[26] J.D. Yoo, K. Ogle, P. Volovitch, The effect of synthetic zinc corrosion products on corrosion of electrogalvanized steel: I. Cathodic reactivity under zinc corrosion products, Corros. Sci. 81 (2014) 11-20.

[27] J.D. Yoo, K. Ogle, P. Volovitch, The effect of synthetic zinc corrosion products on corrosion of electrogalvanized steel: II. Zinc reactivity and galvanic coupling zinc/steel in presence of zinc corrosion products, Corros. Sci. 83 (2014) 32-37.

[28] E. Mena, R.M. Souto, L. Veleva, Early stages of zinc corrosion and runoff process induced by Caribbean sea water, Int. J. Electrochem. Sci. 10 (2015) 7596-7605.

[29] K. Ogle, V. Baudu, L. Garrigues, X. Philippe, Localized electrochemical methods applied to cut edge corrosion, J. Electrochem. Soc. 147 (2000) 3654-3660.

[30] J. Elvins, J.H. Sullivan, J.A. Spittle, D.A. Worsley, Short term predictive testing for cut edge corrosion resistance in zinc–aluminium alloy galvanised steels, Corros. Eng. Sci. Technol. 40 (2005) 43-50.

[31] F. Thébault, B. Vuillemin, R. Oltra, C. Allely, K. Ogle, Protective mechanisms occurring on zinc coated steel cut-edges in immersion conditions, Electrochim. Acta 56 (2011) 8347-8357.

[32] A.Q. Vu, B. Vuillemin, R. Oltra, C. Allély, Cut-edge corrosion of a Zn-55Al-coated steel: A comparison between sulphate and chloride solutions, Corros. Sci. 53 (2011) 3016-3025.

[33] A. Alvarez-Pampliega, M.G. Taryba, K. Van den Bergh, J. De Strycker, S.V. Lamaka, H. Terryn, Study of local Na^+ and Cl^- distributions during the cut-edge corrosion of aluminum rich metal-coated steel by scanning vibrating electrode and micro-potentiometric techniques, Electrochim. Acta 102 (2013) 319-327.

[34] A.G. Marques, J. Izquierdo, R.M. Souto, A.M. Simões, SECM imaging of the cut edge corrosion of galvanized steel as a function of pH, Electrochim. Acta 153 (2015) 238-245.

448 [35] A.G. Marques, M.G. Taryba, A.S. Panão, S.V. Lamaka, A.M. Simões, Application of scanning
449 electrode techniques for the evaluation of iron–zinc corrosion in nearly neutral chloride solutions,
450 Corros. Sci. 104 (2016) 123-131.
451 [36] B.M. Fernández-Pérez, J. Izquierdo, S. González, R.M. Souto, Scanning electrochemical
452 microscopy studies for the characterization of localized corrosion reactions at cut edges of coil-
453 coated steel, J. Solid State Electrochem. 18 (2014) 2983-2992.
454 [37] B.M. Fernández-Pérez, J. Izquierdo, J.J. Santana, S. González, R.M. Souto, Scanning
455 electrochemical microscopy studies for the characterization of localized corrosion reactions at
456 cut edges of painted galvanized steel as a function of solution pH, Int. J. Electrochem. Sci. 10
457 (2015) 10145-10156.
458 [38] Y. Umezawa, P. Bühlmann, K. Umezawa, K. Tohda, S. Amemiya, potentiometric selectivity
459 coefficients of ion-selective electrodes. Part I. Inorganic cations (Technical Report), Pure Appl.
460 Chem. 72 (2000) 1851-2082.
461 [39] S. Thomas, N. Birbilis, M.S. Venkatraman, I.S. Cole, Corrosion of zinc as a function of pH,
462 Corrosion 68 (2012) 015009.
463 [40] T. Prosek, D. Persson, J. Stoulil, D. Thierry, Composition of corrosion products formed on Zn-
464 Mg, Zn-Al and Zn-Al-Mg coatings in model atmospheric conditions, Corros. Sci. 86 (2014) 231-
465 238.
466 [41] J. Izquierdo, A. Kiss, J.J. Santana, L. Nagy, I. Bitter, H.S. Isaacs, G. Nagy, R.M. Souto,
467 Development of Mg^{2+} ion-selective microelectrodes for potentiometric scanning electrochemical
468 microscopy monitoring of galvanic corrosion processes, J. Electrochem. Soc. 160 (2013) C451-
469 C459.
470 [42] A. Kiss, G. Nagy, New SECM scanning algorithms for improved potentiometric imaging of
471 circularly symmetric targets, Electrochim. Acta 119 (2014) 169–174.
472 [43] T.N. Vu, M. Mokaddem, P. Volovitch, K. Ogle, The anodic dissolution of zinc and zinc alloys in
473 alkaline solution. II. Al and Zn partial dissolution from 5% Al-Zn coatings, Electrochim. Acta 74
474 (2012) 130-138.
475 [44] M. Salgueiro Azevedo, C. Allély, K. Ogle, P. Volovitch, Corrosion mechanisms of Zn(Mg,Al)
476 coated Steel: 2. The effect of Mg and Al alloying on the formation and properties of corrosion
477 products in different electrolytes, Corros. Sci. 90 (2015) 482-490.

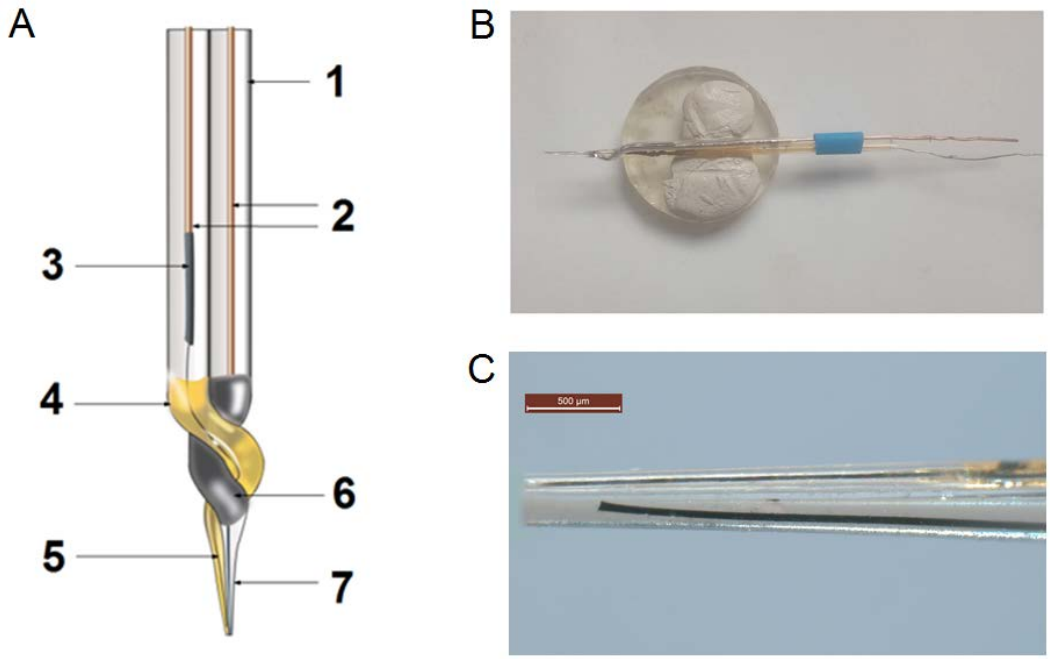

Figure 1. Sketch and (B,C) micrographs of the dual probe for simultaneous potentiometric determination of pH and Zn^{2+} concentration distributions using SECM. 1: double-barrel borosilicate capillary; 2: copper wires; 3: Ag-epoxy; 4: ion selective cocktail; 5: PEDOT coated carbon fiber (∅ = 30 µm); 6: liquid mercury; and 7: antimony fiber. (B) Micrograph of the probe.

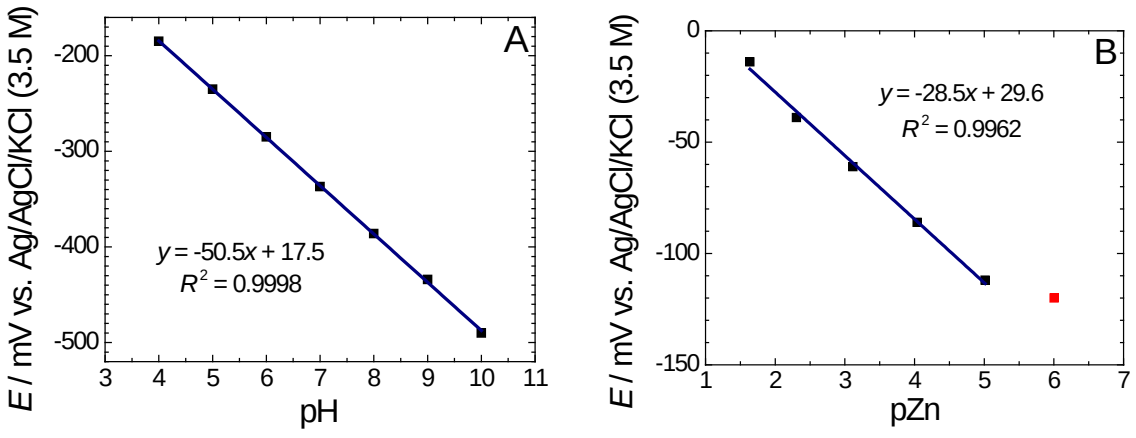

Figure 2. Calibration curves of the Zn^{2+} and pH selective microelectrodes in the dual probe. (A) pH calibration of the antimony electrode; (B) calibration of the Zn^{2+}-ISME.

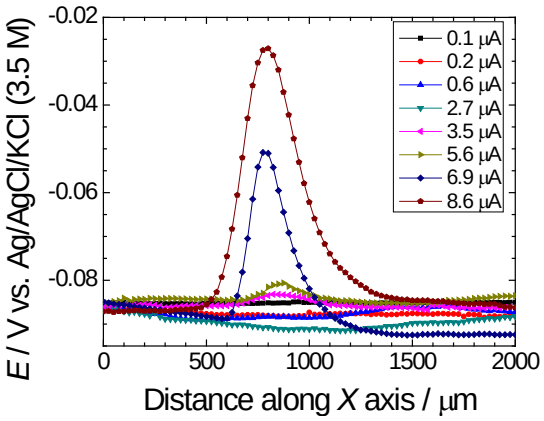

Figure 3. Influence of the electric field generated from a pipette point source on the registered potential of the Zn ISME, scanned at 100 µm height. Currents in the legends indicate the imposed current flowing as a result of the connection in series of kΩ-MΩ resistors and a 6 V battery between the micropipette electrode and a platinum counter electrode.

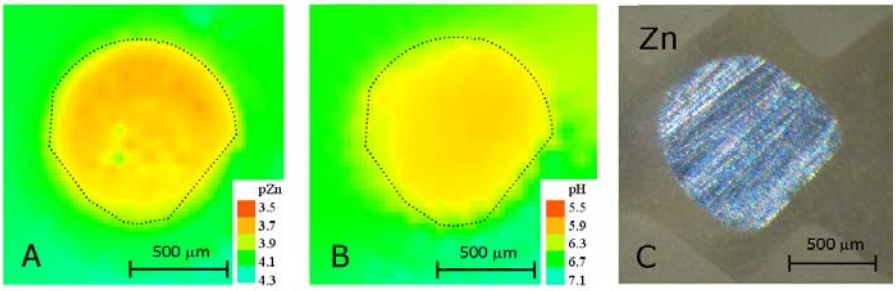

Figure 4. 2D simultaneous Zn^{2+} and pH imaging over the sacrificial anode of the Fe-Zn galvanic couple immersed in 1 mM NaCl. (A) Zn^{2+}distribution obtained with the Zn^{2+} ISME of the dual probe; (B) pH distribution obtained with the Sb/Sb_2O_3 microelectrode of the dual probe; (C) photograph of the Zn wire during the measurements.

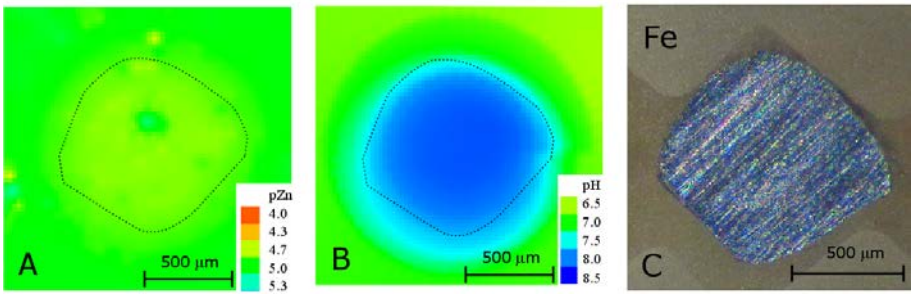

Figure 5. 2D simultaneous Zn^{2+} and pH imaging over the Fe cathode of the Fe-Zn galvanic couple immersed in 1 mM NaCl. (A) Zn^{2+}distribution obtained with the Zn^{2+} ISME of the dual probe; (B) pH distribution obtained with the Sb/Sb_2O_3 microelectrode of the dual probe; (C) photograph of the Fe wire during the measurements.

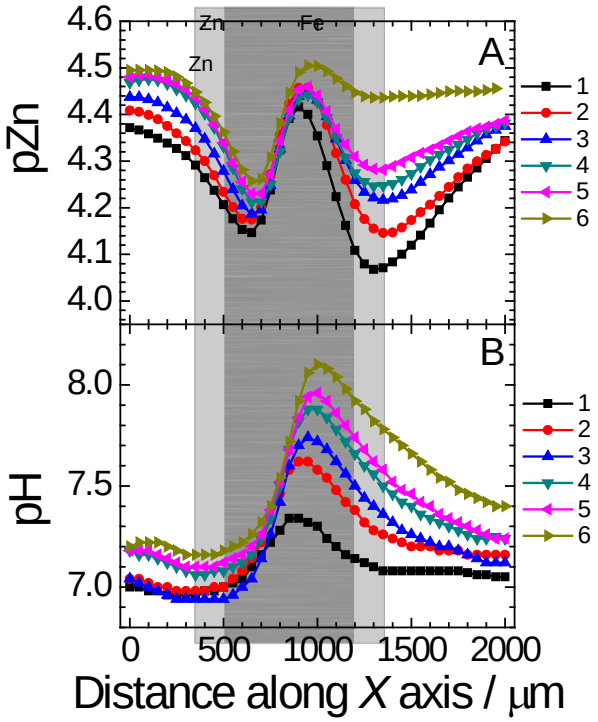

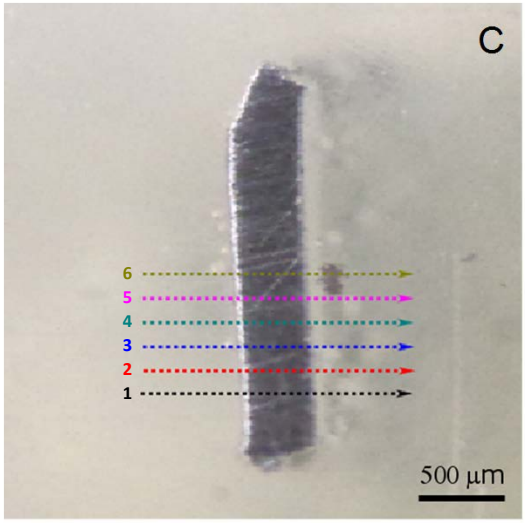

Figure 6. Scan lines recorded during simultaneous measurement of pH and Zn^{2+} distribution above the cut edge of painted galvanized steel immersed in 1 mM NaCl. (A) pZn profiles; (B) pH profiles; (C) micrograph of the exposed cut edge with indication of the approximate location of the line scans presented in (A) and (B). The arrows show the scan direction; the time elapsed between recording the scan lines is 1 minute, starting from the line at the bottom and moving sequentially to the top.

Table 1. Selectivity coefficients of the Zn-ISME determined using the separate solution method (SSM) and comparison with those reported by the supplier of the ionophore.

	Determined by SSM	Reported by Fluka
$\log(K^{pot}_{Zn^{2+},Fe^{2+}})$	-2.02	-2.42
$\log(K^{pot}_{Zn^{2+},Fe^{3+}})$	-2.13	
$\log(K^{pot}_{Zn^{2+},\ Na^{+}})$	-3.24	-3.28